CrystEngComm

PAPER

View Article Online
View Journal | View Issue

Cite this: *CrystEngComm*, 2016, **18**, 8101

Hierarchical core/shell ZnO/NiO nanoheterojunctions synthesized by ultrasonic spray pyrolysis and their gas-sensing performance

Dan Li,[b] Yiqun Zhang,[b] Deye Liu,[b] Shiting Yao,[b] Fengmin Liu,*[ab] Biao Wang,[c] Peng Sun,[b] Yuan Gao,[b] Xiaohong Chuai[b] and Geyu Lu*[ab]

Received 22nd July 2016,
Accepted 19th September 2016

DOI: 10.1039/c6ce01621a

www.rsc.org/crystengcomm

ZnO nanorod arrays decorated with NiO nanosheets on FTO substrates were prepared *via* a simple ultrasonic spray pyrolysis process combined with chemical bath method. The synthesized samples were characterized and analyzed by scanning electron microscopy and X-ray diffraction. The hierarchical and porous morphologies of ZnO/NiO core–shell nanoheterojunctions could be controlled by changing the growth time of NiO sheets. The "oriented attachment" and "self-assembly" crystal growth mechanisms were proposed to explain the formation of the ZnO/NiO nanostructures. Sensors based on the ZnO/NiO heterojunction nanostructure were fabricated and investigated for their ethanol-sensing properties. The result indicated that response was about 180% toward 100 ppm ethanol at an operating temperature of 200 °C. The growth approach in this work offers a new technique for the design and synthesis of transition metal oxide hierarchical nanoarrays which are promising for gas sensing applications.

1. Introduction

During the past few decades, one-dimensional semiconductor oxide nanomaterials, such as nanowires,[1] nanorods[2] and nanotubes (NTs),[3] have attracted extensive attention in view of enhancing performance in electrical nanodevices, such as gas sensors,[4,5] biosensors,[6] solar cells,[7] *etc.* As a special type of 1D structure, zinc oxide,[8–10] one of the most important functional semiconductor materials, with a direct band gap of 3.4 eV and a large exciton binding energy of 60 meV, has attracted intensive research due to its unique properties and versatile applications in chemical sensors.[11–13] To improve the gas sensing properties of ZnO, doping with various materials has been employed to modify its surface properties. For example, the application of noble metal elements, such as Pt,[14–16] Pd,[17] Ag,[18] Au,[19] onto the surface of a metal oxide is a widely accepted technique for enhancing the interaction of reducing gases with the adsorbed oxygen on the metal oxide surface, which has been utilized to improve the gas sensing properties of metal oxide semiconductor based gas sensors. Aside from noble metals, metal oxides have also been used to make heterostructures that enhance sensing properties.[20–22] Metal oxide composites can provide electric junction properties at the interface of heterostructures. Among the many surface doping/composite materials, NiO,[23–26] a p-type semiconductor material with an energy band gap of 4.2 eV, can be used in combination with ZnO to form a heterojunction, which is expected to enhance the response of gas sensors. Nickel oxide nanocones decorated with zinc oxide nanothorns on nickel oxide foil substrates form heterojunctions in the micro region and enhance gas sensing characteristics to NH_3.[27] Novel NiO@ZnO heterostructured NTs were fabricated by the coelectrospinning method with enhanced gas sensing characteristics to H_2S.[28] However, to the best of our knowledge, studies of nickel oxide nanosheets decorated with zinc oxide nanorods on FTO substrates have been rarely reported.

Compared with other synthesis methods, ultrasonic spray pyrolysis (USP)[29,30] and chemical bath deposition (CBD)[31,32] have many advantages such as effective stoichiometry control, excellent homogeneity, relatively low processing temperature and low-cost fabrication for synthesizing materials.

In this paper, we firstly synthesized ZnO nanorods by a USP method on FTO substrate. In order to improve the sensing performance, a ZnO/NiO heterojunction was designed to detect ethanol gas, where NiO nanosheets were implanted onto the surface of ZnO nanorods by CBD. ZnO nanorods decorated with NiO nanosheets have high specific surface area and well-organized structure compared with simple ZnO nanorods. Our growth approach offers a new technique for the design and synthesis of transition metal oxide

[a] *State Key Laboratory of Automotive Simulation and Control, Jilin University Nanling Compus, 5988 Renmin Street, Changchun 130025, China. E-mail: liufm@jlu.edu.cn; Fax: +86 431 85167808*
[b] *State Key Laboratory on Integrated Optoelectronics, College of Electronic Science and Engineering, Jilin University, 2699 Qianjin Street, Changchun 130012, China*
[c] *State Key Laboratory of Luminescence and Application, Changchun Institute of Optics, Fine Mechanics and Physics, Chinese Academy Sciences, Changchun 130033, China*

hierarchical nanoarrays which are promising for gas sensing applications.

2. Experimental

2.1 Growth of pure ZnO nanorods

All chemicals in the experiment were of analytical reagent grade and used without further purification. First, a ZnO seed layer was preferentially deposited by a USP method on the FTO substrate. Then 0.329 g of zinc acetate dihydrate ($Zn(CH3COO)_2{\cdot}2H_2O$) and 0.700 g of hexamethylenetetramine were dissolved in 8 mL deionized water to form a clear precursor solution. Then the precursor solution was sprayed with N_2 carrier gas (500 sccm) and pyrolyzed on the surface of the substrate at 300 °C for 15 min. Subsequently, the precursor solution was changed to a mixture of 0.681 g of zinc chloride ($ZnCl_2$) and 0.1 ml of monoethanolamine, while the deposition time was 2 h. Finally, pure ZnO nanorods were obtained by annealing the above products at 500 °C for 2 h in air.

2.2 Synthesis of hierarchical core/shell ZnO/NiO nanoheterojunctions

NiO nanosheets were dispersed onto the surface of ZnO nanorods by a CBD method. In a typical synthesis, a solution for CBD was prepared by adding 1 mL of aqueous ammonia (25–28%) to a mixture of 20 mL of 1 M nickel sulfate and 16 mL of 0.25 M potassium, the potassium persulfate acting as an oxidant. The ZnO nanorods were immersed into the CBD solution for 10 min, 15 min, and 20 min at 40 °C, the corresponding products being denoted as ZN(a), ZN(b), and ZN(c), respectively. Finally, the samples were rinsed with distilled water and annealed at 350 °C in air for 2 h.[31] Hierarchical core/shell ZnO/NiO nanoheterojunctions were successfully prepared.

2.3 Characterization

X-ray diffraction (XRD) patterns were collected by using a Rigaku TTRIII X-ray diffractometer operated at 40 kV and 200 mA with Cu Kα radiation at a wavelength of 1.5406 Å in the range of 20–80° (2θ) at room temperature. Field emission scanning electron microscopy (FESEM) images were obtained using a JEOL JSM-7500F microscope with an accelerating voltage of 15 kV. X-ray photoelectron spectroscopy (XPS) was conducted with a Kratos AXISHS X-ray photoelectron spectrometer equipped with a standard and monochromatic source (Al KR) operated at 150 W (15 kV, 10 mA). Transmission electron microscopy (TEM) and high-resolution TEM images were obtained with a JEOL JEM-3010 microscope operated at 200 kV. Energy-dispersive X-ray spectroscopy (EDS) data were measured by the TEM attachment.

2.4 Fabrication and measurement of gas sensor

Gas sensors were fabricated as follows: the as-prepared products were scraped off from the FTO substrates and subsequently dispersed in deionized water to form a paste. The paste was coated onto a ceramic tube on which a pair of gold electrodes had been previously printed, and then a Ni–Cr heating wire was inserted in the tube to form a side-heated gas sensor, which allowed for the control of the working temperature. The gas sensing performance of the gas sensor was evaluated by a static test method using an RQ-2 gas-sensing characterization system. The electrical resistance of the sensor in different environmental atmospheres was measured, with atmospheric air being used as the reference gas. The gas response (S) of the sensor is defined as the ratio of R_g/R_a,[33] in which R_g and R_a are the electrical resistance of the sensor in the target gas and atmospheric air.

3. Results and discussion

3.1 Structural and morphological characteristics

Fig. 1 shows the FESEM images of the ZnO/NiO core–shell nanostructures synthesized by combining USP and CBD methods. The pure ZnO nanorods that were grown for 2 h have an average diameter of 300 nm and a length of up to around 5 μm as shown in Fig. 1a.

After CBD, as shown in Fig. 1b–d, ZnO nanorods were partly dissolved during the immersion period and were decorated with NiO nanosheets. For the sample reacted for 10 min, the diameter of the ZnO nanorods hardly changed and a small amount of nanosheets are observed in Fig. 1b. When the reaction was extended to 15 min, the thickness of the nanosheets greatly increased as shown in Fig. 1c. As the reaction was prolonged to 20 min, from Fig. 1d it can be seen that the nanosheet shells are interconnected and fully covered the surface of the ZnO core. The coverage of these nanosheets appeared to be quite uniform. ZnO/NiO nanostructure could be easily controlled by changing the reaction time.

The ZnO core nanorods and NiO shell nanosheets can be easily distinguished from the TEM images. Fig. 2a further demonstrates that the products have a core–shell

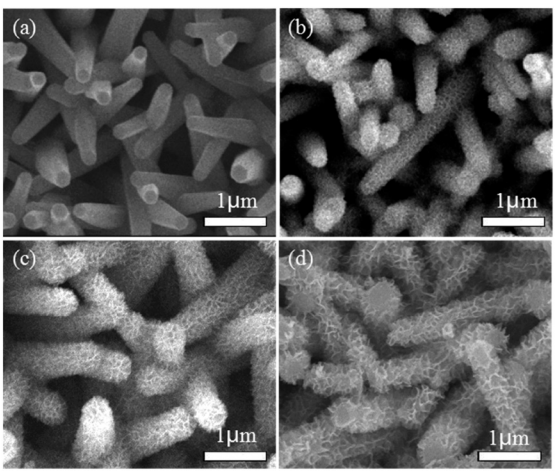

Fig. 1 SEM images of the ZnO/NiO nanostructure fabricated after immersion in nickel sulfate solution for different times: (a) 0 min, (b) 10 min, (c) 15 min, (d) 20 min.

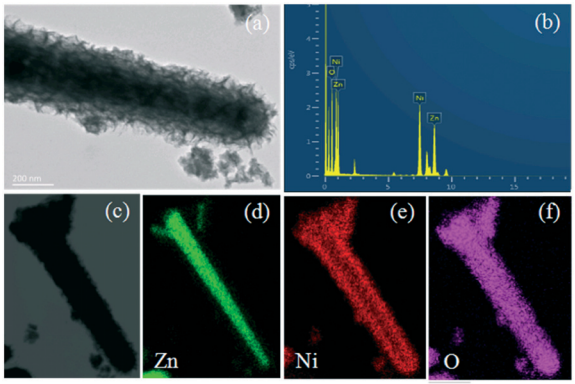

Fig. 2 (a) Typical TEM image of the ZN(a) nanostructure. (b) EDS spectrum of NiO/ZnO nanostructures. (c) TEM image of the ZN(a) nanostructures; (d)–(f) corresponding elemental mapping images of the ZN(a) nanostructures.

nanostructure. Besides the morphology of the ZnO/NiO core–shell nanostructures, a corresponding EDS elemental mapping of Zn, Ni, and O is also shown in Fig. 2b. Fig. 2c–f shows scanning TEM images of a ZnO/NiO core/shell nanostructure. TEM elemental mapping was conducted to clearly confirm the localized presence of Zn in the core area. Ni element is inclined to distribute along the surface of the nanorods in Fig. 2e, showing that Ni element from NiO nanosheets is well dispersed on ZnO nanorods. The results are in good agreement with the above FESEM and TEM results.

The XRD patterns of pure ZnO and ZN(a), ZN(b), and ZN(c) nanostructure samples are shown in Fig. 3. Clearly, it can be seen that all diffraction peaks can be well indexed to a hexagonal wurtzite structure of zinc oxide (JPCDS: 75-566) for the pure ZnO and cubic NiO phase (JCPDS: 2-1216) for ZN(a), ZN(b), and ZN(c) samples. With the CBD time increasing, the peaks of ZnO were weaker and weaker in the patterns of the composites, which means that the ZnO nanorods were partly dissolved and more NiO shells grew on the surface of the ZnO core.

To further illuminate the surface composition and chemical state of elements existing in ZnO/NiO core–shell samples,

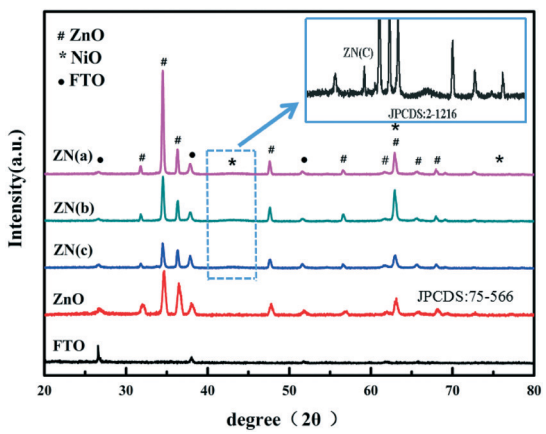

Fig. 3 XRD patterns of pure ZnO and ZnO/NiO nanostructure.

we studied XPS spectra of sample ZN(a). Fig. 4 shows the typical XPS spectra of the ZnO/NiO nanostructure, where Fig. 4a is the survey spectrum and Fig. 4b–e are the high-resolution binding energy spectra with fitting analysis of Zn, Ni and O. For ZN(a) sample in Fig. 4b, there are two symmetric peaks in the Zn 2p region. The peak centered at about 1022 eV corresponds to Zn $2p_{3/2}$, and the other one centered at about 1045 eV is assigned to Zn $2p_{1/2}$. The observed spin–orbit splitting of Zn 2p between Zn $2p_{3/2}$ and Zn $2p_{1/2}$ for the ZN(a) nanostructure is about 23 eV, which is consistent with the corresponding value of pure ZnO, indicating a normal state of Zn^{2+} in ZN(a) sample.[34] In Fig. 4c, the XPS spectrum of Ni $2p_{3/2}$ consists of three components located at about 854 eV, 856 eV and 861 eV respectively,[35] which are all ascribed to Ni–O bond. In addition, the peak at 863 eV is a satellite peak of Ni $2p_{3/2}$, which also proves the existence of Ni^{2+}. In Fig. 4d–e, O 1s is not only from ZnO but also from the NiO shell, and the binding energies of ZN(a) and ZN(c) at about 529.5 eV, 531.5 eV, and 532.8 eV were attributed to lattice oxygen, oxygen-deficient regions, and chemisorbed oxygen species of ZnO/NiO composite, respectively.[36]

3.2 Possible mechanism of formation

In order to reveal the growth process of ZnO/NiO nanostructure and a possible growth mechanism, the study of the morphology evolution of ZnO/NiO core–shell nanostructure with different reaction times has been carried out, as shown in Fig. 5. The nonpolar $\{10\bar{1}0\}$ planes of ZnO crystal structure are parallel to the [0001] direction (*c*-axis), which has lower surface energy and higher stability[10] so that the ZnO grew preferentially along the (0001) direction and the nanorods were generated. After ZnO nanorods were immersed in a chemical water bath of nickel sulfate solution for 2 min, many Ni-based hydroxide nanoparticles nucleated on the surface of the ZnO nanorods to form active sites, which would minimize the interfacial energy barrier for the subsequent growth of Ni-based hydroxide. The combination of these nanoparticles decreased the overall energy by removing

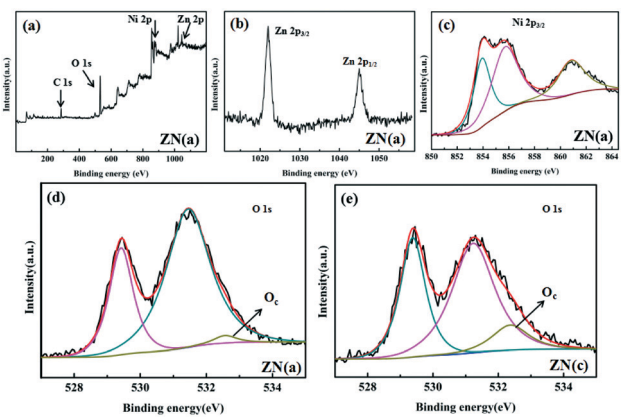

Fig. 4 (a) Survey, (b) Zn 2p, (c) Ni 2p and (d) O 1s high-resolution XPS spectra of sample ZN(a). (e) O 1s high-resolution XPS spectra of sample ZN(c).

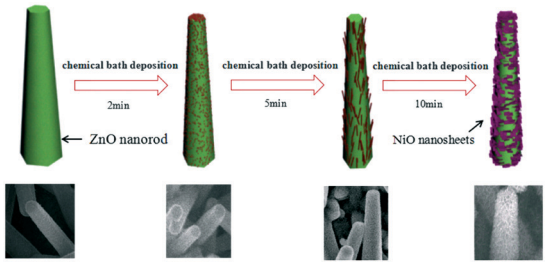

Fig. 5 Schematic illustration of the formation process of ZnO/NiO core–shell nanostructures and corresponding SEM images of the products at various reaction stages after heat treatment.

surface energy which was beneficial for adjacent Ni-based hydroxide nanoparticles to spontaneously self-organize together. The self-organized nanoparticles shared a common crystallographic orientation and formed a planar interface. When the reaction proceeded to 10 min these nanoparticles self-assemble to form large nanosheets and finally generate the core–shell nanostructure. The above hypothesis is supported by examining the morphologies at different growth stages by controlling the reaction time, as can be seen in Fig. 5.

3.3 Gas sensing properties

Gas sensors based on pure ZnO and ZnO/NiO nanostructure samples were fabricated in order to investigate the gas sensing property.

Fig. 6 shows the response of the sensors based on pure ZnO, ZN(a), ZN(b) and ZN(c) toward 500 ppm ethanol, methylethanol, acetone, benzene, toluene and formaldehyde at an operating temperature of 200 °C. The sensors based on ZnO/NiO composites showed enhanced response to ethanol compared with pure ZnO nanorods, especially the sensor based on ZN(c).

Fig. 7 shows the responses of the three sensors to 500 ppm ethanol at operating temperatures from 175 °C to 300 °C. It was obvious that the responses of the tested sensors varied with operating temperature. The response of ZN(c) towards ethanol first increased and reached a maximum at an operating temperature of 200 °C, and then decreased on further increasing the operating temperature. Similar behavior could be observed in the case of the other sensors based on ZnO/NiO composites. Their maximal response appeared at a common temperature, but the values of Zn(c) were much higher than those of ZN(a) and ZN(b). Fig. 8 shows the dynamic response resistances of the sensor based on ZN(c) towards different concentrations of ethanol at an operating temperature of 200 °C. The results indicated that the gas responses increased with an increase of ethanol concentration from 100 ppm to 500 ppm and excellent response and recovery characteristics. The response time and recovery time of the sensor were within about 55 s and 70 s, respectively.

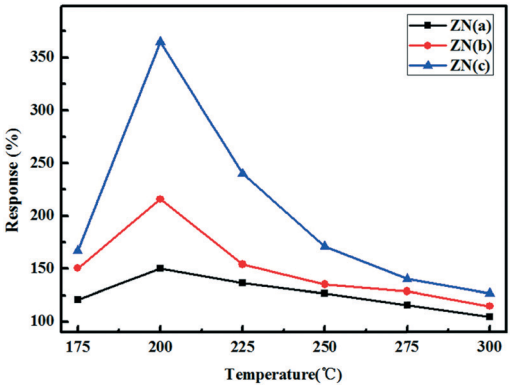

Fig. 7 Relationship between working temperature and response of ZN(a), ZN(b) and ZN(c) sensors to 500 ppm ethanol.

3.4 Gas sensing mechanism

The sensing mechanism of ZnO/NiO composites is likely to be a result of the following factors.

First, the sensing mechanism is related to the change in resistance of the sensor by virtue of the adsorption and desorption processes of oxygen molecules on the surface of oxides. For n-type semiconductor sensors, it involves the interaction between ethanol and the chemisorbed oxygen ions, such as O^{2-}, O^{-} and O^{2-}, on the surface of the crystal. At the beginning of the measurement, when ZnO nanorod sensor is

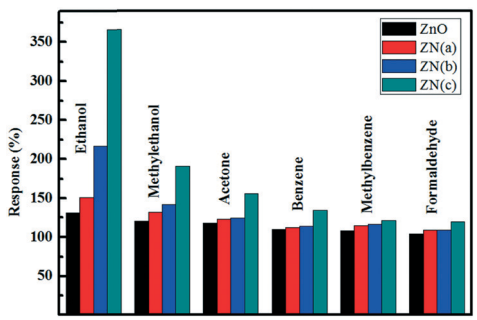

Fig. 6 Selectivities of pure ZnO and ZnO/NiO composites to 500 ppm of various gases at 200 °C.

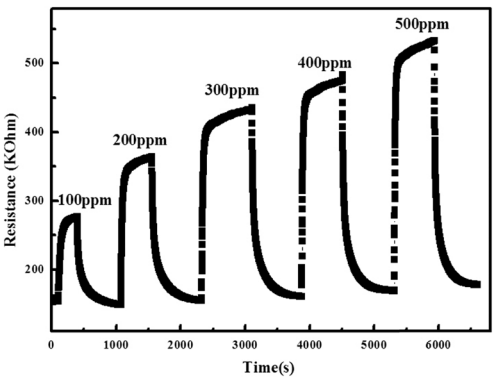

Fig. 8 Responses to different concentrations of ethanol for the sensor based on ZN(c) at 200 °C.

exposed to air, oxygen molecules will adsorb on the surface, forming O^{2-}, O^{-}, O^{2-} species by capturing electrons from the conductance band. As the reductive gas is introduced to the test chamber at an appropriate temperature, such as ethanol in this case, these gas molecules will react with the adsorbed oxygen ions, leading to an increase in concentration of electrons.[27,28] Compared with pure ZnO, the conduction type of ZnO/NiO nanostructures changes from n-type to p-type. And p-type NiO nanosheet shells are interconnected and cover the surface of the ZnO core so that the conduction type and sensing properties are mainly governed by the NiO. When the ZnO/NiO composite sensors are exposed to reductive ethanol, the oxygen ions adsorbed on the surface react with ethanol molecules and release electrons; the released electrons combine with holes in p-type NiO, leading to a decreased concentration of holes and increased resistance.

The reaction between ethanol and ionic oxygen species can take place in two different ways, and the overall reaction can be represented as eqn (1)–(4):[37,38]

$$2C_2H_5OH + 2O_2^- \rightarrow 2C_2H_4O^- + O_2 + 2H_2O + 2e^- \quad (1)$$

$$C_2H_4O^- \rightarrow CH_3CHO + e^- \quad (2)$$

Another way can be seen in the following equations:

$$C_2H_5OH + h^+ + O_2^- \rightarrow CH_3CHO + H_2O \quad (3)$$

$$CH_3CHO + h^+ + O_2^- \rightarrow CO_2 + H_2O \quad (4)$$

In addition, the chemically reductive ethanol molecule may combine with holes in NiO and produce intermediates CH_3CHO which will react with adsorbed oxygen. Overall, the addition of p-type NiO enables the ethanol to react more completely, resulting an increase of ethanol sensitivity.

Second, according to the FESEM and TEM analysis mentioned above, it is reasonable to consider NiO nanosheets as planted on the surface of ZnO nanorods. The morphology of ZnO/NiO core–shell composites was decorated with an amount of porous nanosheets, which can provide a high surface area compared with bare ZnO nanorods and more oxygen can be adsorbed on the surface of the oxide.

Third, the enhancement of sensitivity to ethanol could be ascribed to the formation of n–p junctions between n-type ZnO and p-type NiO. According to the XPS and TEM analyses mentioned above, it is reasonable to consider p-type NiO nanosheets as planted on the surface of ZnO nanorods and thus many p–n junctions are generated near the interface between ZnO and NiO. When the heterostructure sensor is exposed to air at a high temperature, the resistance of the ZnO/NiO in air will be even higher than without the heterojunction due to the depletion region at the heterojunction interface; the corresponding resistance in air increased from 115 kΩ to 155 kΩ.[39,40] The increase of resistance demonstrated that n–p heterojunctions were successfully incorporated. The electrons transfer from n-type ZnO to p-type NiO while the holes transfer from NiO to ZnO until the system obtains equalization at the Fermi level, which will result in the formation of a hole depletion layer and the increase in the amount of the chemisorbed oxygen species.[41] The amount of chemisorbed oxygen species (O_C) can be approximately obtained from XPS spectra. The relative percentage of O_C was approximately 1.8% in ZN(a) sample, while it was 10.6% in ZN(c) sample from Fig. 4d and e; the content of O_C component was greatly increased. This indicated that the gas sensing properties were closely related to the chemisorbed oxygen. The increase of O_C component means that more surface chemisorbed oxygen species could participate in the oxidation–reduction reaction occurring on the surface of the sensing materials and thus cause a larger change in sensor resistance.[42]

4. Conclusion

In summary, ZnO/NiO hierarchical core/shell ZnO/NiO nanostructures were successfully synthesized *via* a simple ultrasonic spray pyrolysis and chemical water bath method. The NiO nanosheet shells were interconnected and fully covered the surface of the ZnO core. The time-dependent morphology evolution of ZnO/NiO samples was studied in detail, which was used to explore the formation mechanism of such a novel structure. The resulting ZnO/NiO nanostructure displayed enhanced gas-sensing properties compared to pure ZnO nanorods. Also, the possible sensing mechanism of the ZnO/NiO nanostructure when sensing ethanol was discussed. The excellent properties of the ZnO/NiO composite material mean it is a promising candidate for sensing applications for ethanol.

Acknowledgements

This research was supported by the National Nature Science Foundation of China (no. 61134010, 61327804, 61474057 and 61520106003), National High-Tech Research and Development Program of China (863 Program, no. 2014AA06A505), Program for Chang Jiang Scholars and Innovative Research Team in University (no. IRT13018).

References

1 W. Wang, T. L. Li, H. M. Wong, P. Chu, R. Kao, S. Wu, F. Leung, T. M. Wong, M. To, K. Cheung and K. Yeung, Development of novel implants with self-antibacterial performance through in-situ growth of 1D ZnO nanowire, *Colloids Surf., B*, 2016, **141**, 623–633.

2 G. Y. Lu, J. Xu, J. B. Sun, Y. S. Yu, Y. Q. Zhang and F. M. Liu, UV-enhanced room temperature NO_2 sensor using ZnO nanorod modified with SO_2 nanoparticles, *Sens. Actuators, B*, 2012, **162**, 82–88.

3 Y. F. Cui, C. Wang, S. J. Wu, Y. Liu and T. M. Wang, Preparation and photocatalytic activity of ZnO/Fe_2O_3 nanorod arrays and ZnO/NiO nanotube arrays, Chinese Physical Society, 2012, vol. 3, p. 037201.

4 Z. S. Hosseini, A. Irajizad and A. Mortezaali, Room temperature H_2S gas sensor based on rather aligned ZnO nanorods with flower-like structures, *Sens. Actuators, B*, 2015, **207**, 865–871.
5 C. Dong, L. Wang and G. Chen, Facile synthesis of CuO micro-sheets over Cu foil in oxalic acid solution and their sensing properties towards n-butanol, *J. Phys. Chem. C*, 2016, **4**, 985–990.
6 H. Q. Zhao, S. P. Yang, N. N. Ding, L. Qin, G. H. Qiu, J. X. Chen, W. H. Zhang, W. H. Chen and T. S. A. Hor, A zwitterionic 1D/2D polymer co-crystal and its polymorphic sub-components: a highly selective sensing platform for HIV ds-DNA sequences, The Royal Society of Chemistry, 2016, vol. 45, pp. 5092–5100.
7 A. Kumar, A. Madaria and C. Zhou, Growth of aligned single-crystalline rutile TiO_2 nanowires on arbitrary substrates and their application in dye-sensitized solar cells, *J. Phys. Chem. C*, 2010, **114**, 7787–7792.
8 G. K. Mani and J. B. Rayappan, Novel and facile synthesis of randomly interconnected ZnO nanoplatelets using spray pyrolysis and their room temperature sensing characteristics, *Sens. Actuators, B*, 2014, **198**, 125–133.
9 D. Y. Son, K. Bae, H. S. Kim and N. G. Park, Effects of seed layer on growth of ZnO nanorod and performance of perovskite solar cell, *J. Phys. Chem. C*, 2015, **119**, 10321–10328.
10 Y. X. Cai, X. W. Li, P. Sun, B. Wagn, F. M. Liu, P. F. Cheng, S. S. Du and G. Y. Lu, Ordered ZnO nanorod array film driven by ultrasonic spray pyrolysis and its optical properties, *Mater. Lett.*, 2013, **112**, 36–38.
11 J. Xu, Y. S. Yu, X. X. He, J. B. Sun, F. M. Liu and G. Y. Lu, Synthesis of hierarchical ZnO orientation-ordered film by chemical bath deposition and its gas sensing properties, *Mater. Lett.*, 2012, **81**, 145–147.
12 O. Dimitrov, D. Nesheva, V. Blaskov, I. Stambolova, S. Vassilev, Z. Levi and V. Tonchev, Gas sensitive ZnO thin films with desired (002) or (100) orientation obtained by ultrasonic spray pyrolysis, *Mater. Chem. Phys.*, 2014, **148**, 712–719.
13 W. Li, N. Chen and X. Xing, A high-performance n-butanol gas sensor based on ZnO nanoparticles synthesized by a low temperature solvothermal route, The Royal Society of Chemistry, 2015, vol. 5, pp. 54372–54378.
14 N. Tamaekong, C. Liewhiran, A. Wisitsoraat and S. Phanichphant, Sensing Characteristics of Flame-Spray-Made Pt/ZnO Thick Films as H_2 Gas Sensor, *Sensors*, 2009, **9**, 6652–6669.
15 Y. J. Kwon, H. G. Na, S. Y. Kang, S. W. Choi, S. Kim and W. Kim, Selective detection of low concentration toluene gas using Pt-decorated carbon nanotubes sensors, *Sens. Actuators, B*, 2016, **227**, 157–168.
16 C. Dong, X. Liu and X. Xiao, Combustion synthesis of porous Pt-functionalized SnO_2 sheets for isopropanol gas detection with a significant enhancement in response, *J. Mater. Chem. A*, 2014, **2**, 20089–20095.
17 S. Kim, Y. Lee, A. Gu, C. You, K. Oh, S. Lee and Y. Im, Synthesis of vertically conformal ZnO/CuO core–Shell nanowire arrays by electrophoresis-assisted electroless deposition, *J. Phys. Chem. C*, 2014, **118**, 7377–7385.
18 C. Dong, X. Liu, B. Han, S. Deng, X. Xiao and Y. Wang, Nonaqueous synthesis of Ag-functionalized In_2O_3/ZnO nanocomposites for highly sensitive formaldehyde sensor, *Sens. Actuators, B*, 2016, **224**, 193–200.
19 Y. F. Bing, Y. Zeng and S. R. Feng, Multistep assembly of Au-loaded SnO_2 hollow multilayered nanosheets for high-performance CO detection, *Sens. Actuators, B*, 2016, **227**, 362–372.
20 H. Kim, A. Katoch, S.-H. Kim and S. S. Kim, Chemiresistive sensing behavior of SnO_2 (n)–Cu_2O (p) core–shell nanowires, *ACS Appl. Mater. Interfaces*, 2015, **7**, 15351–15358.
21 C. Wang, X. Y. Cheng, X. Zhou, P. Sun, X. L. Hu, K. Shimanoe, G. Y. Lu and N. Yamazoe, Hierarchical α-Fe_2O_3/NiO composites with a hollow structure for a gas sensor, *ACS Appl. Mater. Interfaces*, 2014, **6**, 12031–12037.
22 M. M. Rahman, A. Jamal, S. B. Khan and M. Faisal, CuO codoped ZnO based nanostructured materials for sensitive chemical sensor applications, *ACS Appl. Mater. Interfaces*, 2011, **3**, 1346–1351.
23 J. M. Choi, J. H. Byun and S. S. Kim, Influence of grain size on gas-sensing properties of chemiresistive p-type NiO nanofibers, *Sens. Actuators, B*, 2016, **227**, 149–156.
24 A. Khalil, J. J. Kim, H. L. Tuller, G. C. Re and R. Hashakeh, Gas sensing behavior of electrospun nickel oxide nanofibers: effect of morphology and microstructure, *Sens. Actuators, B*, 2016, **227**, 54–64.
25 Q. Li, N. Chen and X. Xing, NiO nanosheets assembled into hollow microspheres for highly sensitive and fast responding VOC sensors, The Royal Society of Chemistry, 2015, vol. 5, pp. 80786–80792.
26 C. Dong, X. Xiao and G. Chen, Porous NiO nanosheets self-grown on alumina tube using a novel flash synthesis and their gas sensing properties, The Royal Society of Chemistry, 2015, vol. 5, pp. 4880–4885.
27 J. Wang, P. Yang and X. W. Wei, High-performance, room-temperature, and no-humidity-impact ammonia sensor based on heterogeneous nickel oxide and zinc oxide nanocrystals, *ACS Appl. Mater. Interfaces*, 2015, **7**, 3816–3824.
28 L. Xu, R. F. Zheng, S. H. Liu, J. Song, J. S. Chen, B. Dong and W. Song, NiO@ZnO heterostructured nanotubes: coelectrospinning fabrication, characterization, and highly enhanced gas sensing properties, *Inorg. Chem.*, 2012, **51**, 7733–7740.
29 G. K. Mani and J. B. B. Rayappan, ZnO nanoarchitectures: ultrahigh sensitive room temperature acetaldehyde sensor, *Sens. Actuators, B*, 2016, **223**, 343–351.
30 E. Kaber, T. Raadik and T. Dedova, Photoluminescence of spray pyrolysis deposited ZnO nanorods, *Nanoscale Res. Lett.*, 2011, **6**, 351–359.
31 Y. D. J. Jamasali and A. C. Alguno, Chemical bath deposition growth and characterization of zinc oxide nanostructures on plain and platinum-coated glass substrates for hydrogen peroxide gas sensor application, *Mater. Sci. Eng.*, 2015, **79**, 012016.

32 K. Emphasis, R. Vequizo, M. K. Odarve, J. Gambe and A. Alguno, Growth of zinc oxide nanostructures on glass substrates for ethanol gas sensor application, *Mater. Sci. Eng., A*, 2015, **79**, 012008.

33 J. W. Yoon, H. Kim and I. Kim, Electronic sensitization of the response to C_2H_5OH of p-type NiO nanofibers by Fe doping, *Nanotechnology*, 2013, **24**, 444005–4444013.

34 M. Yao, Z. Hu and Y. Liu, 3D hierarchical mesoporous roselike NiO nanosheets for high-performance supercapacitor electrode, *J. Alloys Compd.*, 2015, **648**, 414–418.

35 J. Ma, Y. X. Cai, X. W. Li, S. T. Yao, Y. Liu, F. Liu and G. Y. Lu, Synthesis of hierarchical $ZnO/ZnFe_2O_4$ nanoforests with enhanced gas-sensing performance toward ethanol, *CrystEngComm*, 2015, **17**, 8683.

36 B. Zhao, X. K. Ke, J. H. Bao, C. L. Wang, L. Dong, Y. W. Chen and H. Chen, Synthesis of flower-like NiO and effects of morphology on its catalytic properties, *J. Phys. Chem. C*, 2009, **113**, 14440–14447.

37 Y. B. Zhang, J. Yin, L. Li, L. Zhang and L. Bie, Enhanced ethanol gas-sensing properties of flower-like p-CuO/n-ZnO heterojunction nanorods, *Sens. Actuators, B*, 2014, **202**, 500–507.

38 P. P. Sahay, S. Tewari, S. Jha and M. Shamsuddin, Sprayed ZnO thin films for ethanol sensors, *J. Mater. Sci.*, 2005, **40**, 4791–4793.

39 D. Chen, X. Hou, H. Wen, Y. Wang, H. Wang, X. Li, R. Zhang, H. Lu, H. Xu, S. Guan, J. Sun and L. Gao, The enhanced alcohol-sensing response of ultrathin WO_3 nanoplates, *Nanotechnology*, 2010, **21**, 035501.

40 D. Ju, H. Xu, Q. Xu, H. Gong, Z. W. Qiu, J. Guo, J. Zhang and B. Q. Cao, High triethylamine-sensing properties of NiO/SnO_2 hollow sphere P–N heterojunction sensors, *Sens. Actuators, B*, 2015, **215**, 39–44.

41 H. Kim, H. M. Jeong, T. Kim, J. H. Chung, Y. C. Kang and J. H. Lee, Enhanced ethanol sensing characteristics of In_2O_3-decorated NiO, *ACS Appl. Mater. Interfaces*, 2014, **6**, 18197–18204.

42 C. Wang, X. B. Cui, J. Y. Liu, X. Zu, X. Y. Cheng, P. Sun, X. L. Hu, X. W. Li, J. Zheng and G. Y. Lu, Design of superior ethanol gas sensor based on Al-doped NiO nanorod-flowers, *ACS Sens.*, 2016, **1**, 131–136.